doi:10.1016/j.jmb.2008.08.029 J. Mol. Biol. (2008) 383, 588–602

JMB

Available online at www.sciencedirect.com

ScienceDirect

ELSEVIER

Crystallographic Structure of Phosphofructokinase-2 from *Escherichia coli* in Complex with Two ATP Molecules. Implications for Substrate Inhibition

Ricardo Cabrera[1], Andre L. B. Ambrosio[2], Richard C. Garratt[2], Victoria Guixé[1] and Jorge Babul[1]*

[1]*Departamento de Biología, Facultad de Ciencias, Universidad de Chile, Casilla 653, Santiago, Chile*

[2]*Centro de Biotecnologia Molecular Estrutural, Instituto de Física de São Carlos, Universidade de São Paulo, São Paulo, Brazil*

Received 27 April 2008; received in revised form 10 August 2008; accepted 14 August 2008
Available online 22 August 2008

Phosphofructokinase-1 and -2 (Pfk-1 and Pfk-2, respectively) from *Escherichia coli* belong to different homologous superfamilies. However, in spite of the lack of a common ancestor, they share the ability to catalyze the same reaction and are inhibited by the substrate MgATP. Pfk-2, an ATP-dependent 6-phosphofructokinase member of the ribokinase-like superfamily, is a homodimer of 66 kDa subunits whose oligomerization state is necessary for catalysis and stability. The presence of MgATP favors the tetrameric form of the enzyme. In this work, we describe the structure of Pfk-2 in its inhibited tetrameric form, with each subunit bound to two ATP molecules and two Mg ions. The present structure indicates that substrate inhibition occurs due to the sequential binding of two MgATP molecules per subunit, the first at the usual site occupied by the nucleotide in homologous enzymes and the second at the allosteric site, making a number of direct and Mg-mediated interactions with the first. Two configurations are observed for the second MgATP, one of which involves interactions with Tyr23 from the adjacent subunit in the dimer and the other making an unusual non-Watson-Crick base pairing with the adenine in the substrate ATP. The oligomeric state observed in the crystal is tetrameric, and some of the structural elements involved in the binding of the substrate and allosteric ATPs are also participating in the dimer–dimer interface. This structure also provides the grounds to compare analogous features of the nonhomologous phosphofructokinases from *E. coli*.

Keywords: phosphofructokinases from *E. coli*; substrate inhibition; protein–nucleotide interactions; intersubunit interactions; analogous enzymes

Edited by M. Guss

Introduction

The interconversion between fructose-6-P and fructose-1,6-bisP is one of the three points of central metabolism where the occurrence of substrate cycling results in the net hydrolysis of ATP.[1] As a consequence, regulatory properties coherent with the prevention of the metabolic uncoupling resulting from substrate cycling are expected to be found in the enzymes involved at these critical points of the metabolic network.

The two phosphofructokinases from *Escherichia coli*, phosphofructokinase-1 and -2 (Pfk-1 and Pfk-2, respectively), have been described as showing substrate inhibition by MgATP at low concentrations of the co-substrate fructose-6-P.[2,3] However, a mutant form of Pfk-2 (Tyr23Asp) insensitive to substrate inhibition leads to a reduction in the growth rate of the bearing strain, when cultured on a gluconeogenic carbon source, due to substrate cycling.[4] Since Pfk-1 and Pfk-2 belong to different homologous groups (CATH superfamilies 3.40.50.450 and 3.40.1190.20, respectively), it is rather surprising how independent lineages of phosphoryl transferases have evolved protein–ligand interactions that are congruent not only with specificity towards the same donor–

*Corresponding author. E-mail address: jbabul@uchile.cl.
Present address: A. L. B. Ambrosio, Veterinary Medical Center, Cornell University, Ithaca, NY 14853, USA.

Abbreviations used: Pfk-1, phosphofructokinase-1; Pfk-2, phosphofructokinase-2; SAXS, small-angle X-ray scattering; AIRs, aminoimidazole riboside; PDB, Protein Data Bank; ASA, accessible surface area.

acceptor pair but also with interactions that result in inhibition by the same substrate.

Pfk-1 is a homotetrameric enzyme whose structure in complex with its products at the active site, with MgADP at the allosteric site, as well as the apo form has been solved by X-ray crystallography.[5,6] The subunits consist of two domains with a central β-sheet surrounded by α-helices. Each subunit contributes with complementary parts of two active sites and two allosteric sites, and the complete tetramer is required for all eight sites. The allosteric site in Pfk-1 is not involved in the MgATP inhibition but binds effectors such as ADP, GDP (activators), and PEP (inhibitor).[7] MgATP inhibition in Pfk-1 is originated by the allosteric communication between the active sites in the oligomer, according to the model of Johnson and Reinhart.[8] Substrate binding antagonism, as observed for Pfk-1,[9] when manifested between active sites on an oligomeric enzyme, will cause substrate inhibition with MgATP acting in the active site of one subunit as an allosteric inhibitor of fructose-6-P affinity of another subunit in the oligomer. Johnson and Reinhart demonstrated with the use of hybrid oligomers that a tetrameric Pfk-1 with only one functional active site is not able to show substrate inhibition, highlighting the importance of intersubunit interactions for the regulation mechanism of this enzyme.[8]

In an alternative view, Wang and Kemp proposed that ATP inhibition results from substrate antagonism coupled with a steady-state random mechanism wherein the high rate of catalysis does not permit equilibration of the binding of the substrates.[10] Correlation between decreased k_{cat} (which allows the equilibration of the binding events) and absence of substrate inhibition in a number of kinetic studies with alternate substrates and mutant forms of the enzyme gives support to this view.

The homodimeric Pfk-2 is a member of the ribokinase family of sugar kinases.[11] In this family, a major cluster of phosphosugar kinases, including Pfk-2, 1-phosphofructokinases, and tagatose-6-P kinases, is observed separated from ribokinases and fructokinases. The first X-ray structure determined was that of *E. coli* ribokinase.[12] Subsequently, structural comparison has allowed the inclusion of adenosine kinases,[13,14] as well as nucleoside kinases,[15] aminoimidazole riboside (AIRs) kinase,[16] and 2-keto-3-deoxygluconate kinases[17,18] within the ribokinase family. More recently, the structure of 6-phosphotagatose kinase from *Staphylococcus aureus* was also solved[19] and structures of 1-phosphofructokinases have been deposited in the Protein Data Bank (PDB),[20] but without an associated publication. All these enzymes have in common a two-domain organization, with a large domain having the architecture of an α/β/α three-layer sandwich and a small domain composed of a four-stranded β-sheet that interacts with the corresponding domain of a second subunit in the case of homodimeric structures. In the monomer members of the ribokinase family, the presence of additional secondary-structure elements in the small domain prevents the β-sheet interactions. The active site lies in the cleft formed by both the large and small domains with the site for the sugar lying near the hinge between the domains and the site for ATP lying distal to this hinge.

More distant members show differences in the presence/absence of secondary-structure elements and domains, as well as the connectivity between them. Extending to the superfamily level, homologues include kinases that phosphorylate a variety of hydroxymethyl-bearing substrates, including sugars and coenzymes, using either ATP or ADP as the phosphoryl donor.

An allosteric site for potassium has been observed in ribokinase and AIRs kinase, lying near the ATP substrate site at the active site.[16] In the case of Pfk-2, biochemical evidence indicates that MgATP inhibition is due to its binding at an allosteric site, which also causes the formation of tetramers.[21–23] Models for the tetrameric arrangement together with structural changes involving the relative orientation of domains were proposed from studies using comparative modeling combined with small-angle X-ray scattering (SAXS) measurements.[24] However, there remains a dearth of detailed information concerning the structure of the enzyme at higher resolution, such as the location of the allosteric site, which has hindered a fuller understanding of the mechanism of the allosteric inhibition by ATP.

Pfk-2 has been crystallized in its tetrameric ATP-bound form.[25] In this work, we describe the crystal structure of this complex at a resolution of 1.98Å solved by molecular replacement, using 6-phosphofructokinase from *Bacillus halodurans* as the search model. Electron density for two ATP molecules and two Mg ions is observed in each subunit. One of the ATPs occupies the usual site for the phosphoryl donor in other enzymes of the superfamily while the second (allosteric) ATP interacts with the first and with protein residues from the two subunits that compose the native dimer. Two configurations are observed for the adenosine moiety of the allosteric ATP, one in which the adenine is interacting with Tyr23 from the partner subunit in the dimer and the other interacting via non-Watson-Crick hydrogen bonds with the adenine of the ATP substrate. The proximity of the allosteric and active sites described in this work is a general novel finding for allosteric enzymes. Furthermore, within the ribokinase-like superfamily, this is the first structural description of an ATP-dependent 6-phosphofructokinase, as well as the first reported allosteric site for ATP. These findings will allow for a better understanding of the mechanism of inhibition of Pfk-2 by ATP, as well as its comparison with the corresponding mechanism of the nonhomologue Pfk-1 from *E. coli*.

Results

Overall structure of the monomer

The overall structure of the Pfk-2 subunit consists of two domains: a major three-layered α/β/α

sandwich domain, characteristic of the ribokinase-like superfamily, and a second smaller four-stranded β-sheet domain (Fig. 1a). The active site is located in a shallow groove stretching along the C-terminal edge of the central β-sheet in the major domain. In other members of the ribokinase family, the minor domain has been described as a lid that covers the active site.

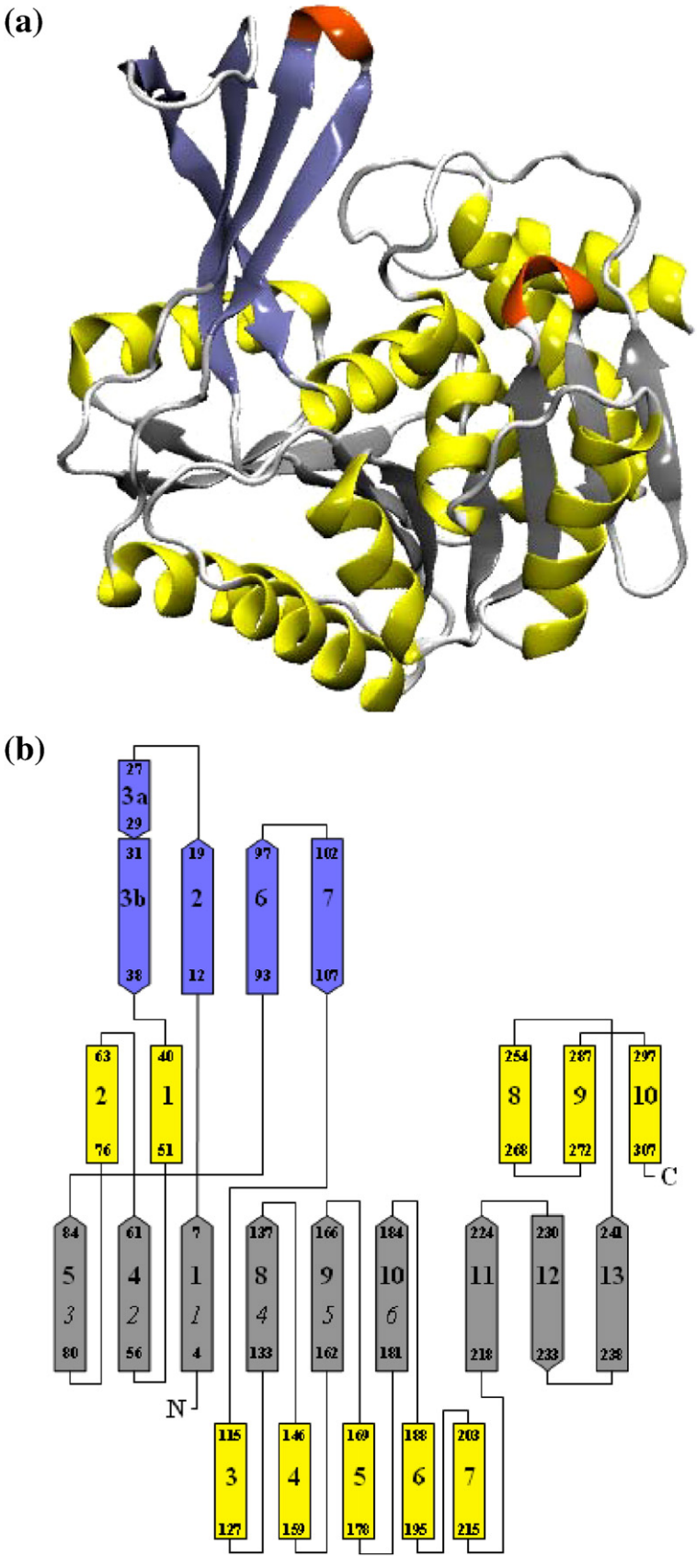

Fig. 1. Structure of the Pfk-2 monomer. (a) Cartoon representation. α-Helices are colored yellow, β-strands in blue (minor domain sheet) and gray (major domain sheet), and loops in white. Loops having the hydrogen-bonding pattern of a 3_{10}-helix are colored orange. (b) Topology diagram. α-Helices shown as rectangles and β-strands shown as arrows are color coded according to (a). Each secondary-structure element is labeled with its designator number and with its beginning and ending sequence number. The first six strands in the major domain are secondarily labeled with the Rossmann ordering number in italics. These strands together with α-helices 1, 2, 3, 4, and 5 constitute the Rossmann module. The β-meander module includes helices 6, 7, 8, 9, and 10 and strands 11, 12, and 13.

The central β-sheet in the major domain shows the typical right-handed twist and is composed of nine strands with the topology β5↑-β4↑-β1↑-β8↑-β9↑-β10↑-β11↑-β12↓-β13↑, surrounded by five α-helices on each side (Fig. 1b). Helices α3, α4, and α5 and the consecutive helices α6 and α7 flank one side of the β-sheet, while helices α1 and α2 and the consecutive helices α8, α9, and α10 are located on the opposite side. Two hydrogen bonds characteristic of a short 3_{10}-helix are observed in the loop connecting β11 and β12 (Fig. 1a).

As first recognized by Sigrell *et al.* the first six strands within the major domain of ribokinase (together with its associated α-helices) have the topology of the Rossmann fold.[12] Pfk-2 follows the same pattern: two βαβαβ motifs (β1α1β4α2β5 and β8α4β9α5β10) connected by a helix linker (α3) that reverses the strands' order in the sheet (Fig. 1b). The major domain is completed by the sequence of secondary-structure elements α_2–β_3–α_3, with the strands forming a β-meander. Most of the enzyme–nucleotide interactions are made by residues in this region of the major domain (see Discussion). It is convenient therefore to describe the major domain as being composed of two modules: the Rossmann module and the β-meander module.

The β-sheet minor domain is composed of two pairs of consecutive antiparallel strands with the topology β3↓-β2↑-β6↑-β7↓ (Fig. 1b). Strands 2 and 3 and strands 6 and 7 are inserted after the first and third strands of the Rossmann module, respectively. In the loop connecting strands 6 and 7, hydrogen bonding characteristic of a 3_{10}-helix is observed (Fig. 1a). Strand 3 has a β-bulge[26] resulting in the splitting of the strand into two halves, indicated as 3a and 3b, in agreement with the original description of *E. coli* ribokinase.[12]

Intersubunit interactions

Pfk-2 elutes as a tetramer in the presence of 1mM MgATP in size-exclusion experiments.[27] A homodimer is observed in the asymmetric unit, which makes extensive contacts with a symmetry-related mate (Fig. 2), forming what appears to be the tetramer under the abovementioned conditions. Intersubunit contacts are found to different extents between the minor domains of all four subunits. Extensive intersubunit contacts are made between the major domains of juxtaposed subunits in adjacent dimers. The subunits in the tetramer are related by 222 (D_2) symmetry, as expected for a tetramer built from two dimers, and they are designated as A, B, C, and D. In Fig. 2, the molecular dyad axes are designated *p*, *q*, and *r*, where *p* corresponds to the noncrystallographic dyad relating the monomers of the asymmetric unit and lies in the *bc* plane of the unit cell, 11° from the *c*-axis. The

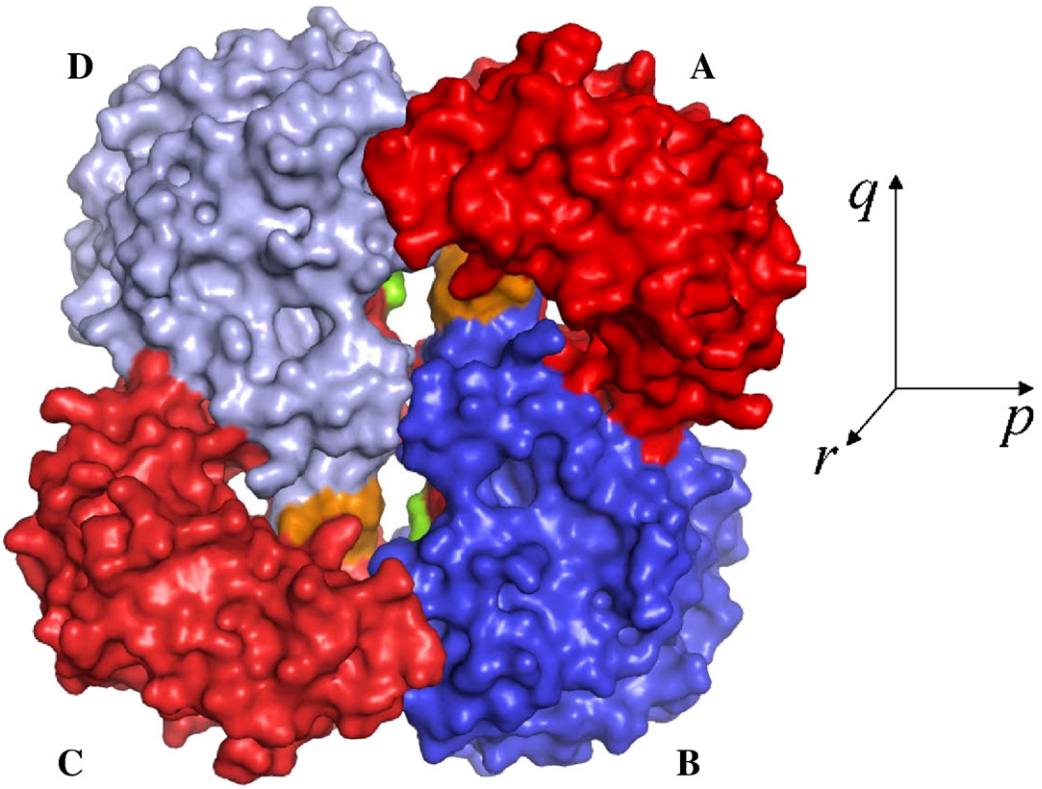

Fig. 2. Symmetry relationships between the subunits. Subunits labeled as A and B correspond to the homodimer seen in the asymmetric unit. The noncrystallographic axis *p* relates these subunits. The dimer formed by the subunits labeled as C and D is related to the AB dimer by the *q*-axis. The axis *r* completes the orthogonal system relating A and C, as well as B and D. Additionally, locations of the ATP molecules are indicated in orange and green.

q-axis corresponds to the crystallographic *a*-axis of the unit cell, relating the two dimers of the tetramer with subunit A mapping to D and subunit B mapping to C. Finally, the noncrystallographic axis *r* relates subunit A to C and subunit B to D.

The β-sheets from the minor domain of each subunit of the dimer are placed face to face with the strand directions, making an approximate right angle, in agreement with the general model for orthogonal β-sheet packing.[28] The presence of a

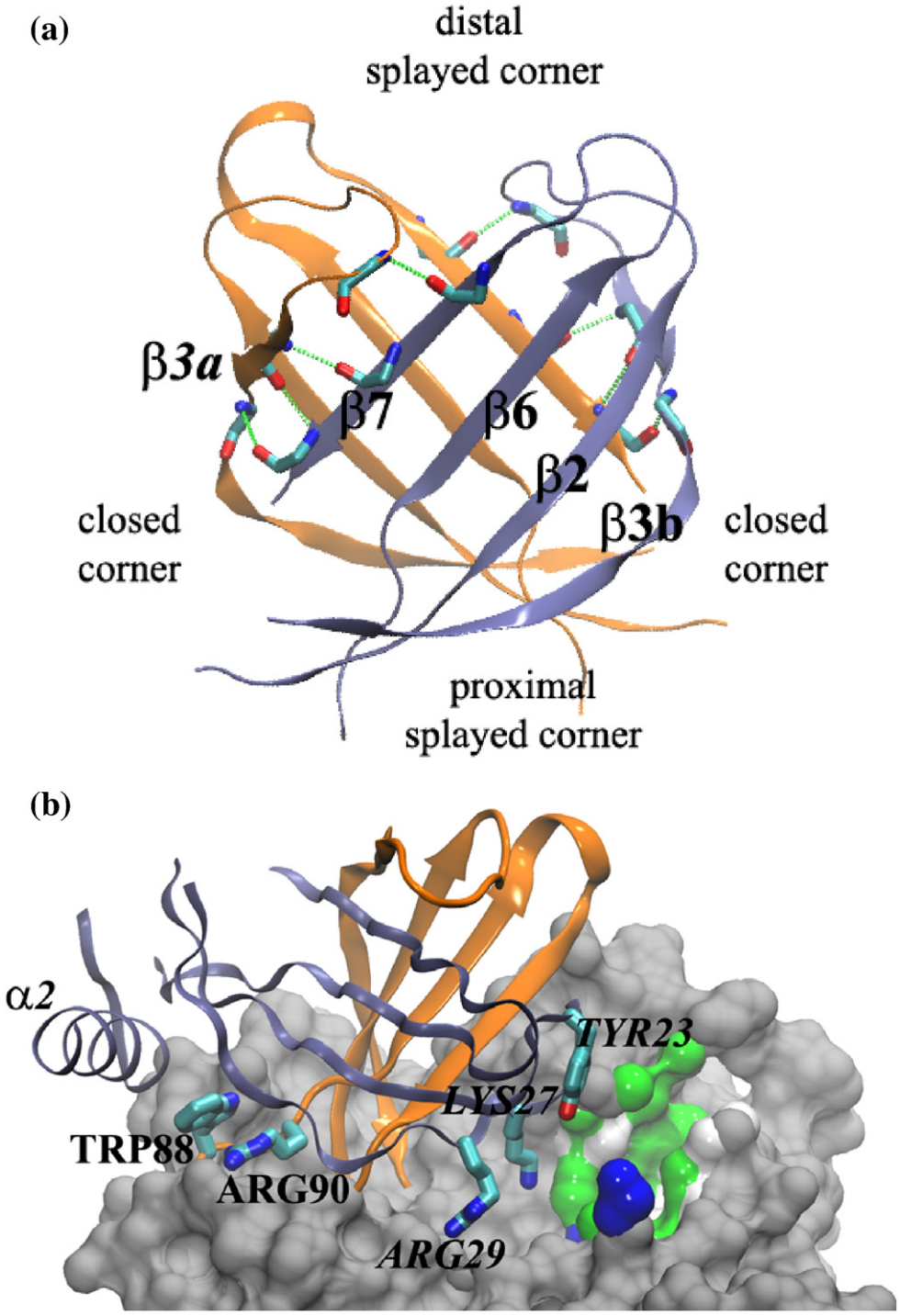

Fig. 3. Structural features of the eight-stranded flattened barrel domain. (a) Orthogonal packing of the four-stranded β-sheets from each subunit of the dimer in the asymmetric unit. Chains from subunits A and B are colored orange and blue, respectively. Hydrogen bonds in the parallel ladder formed between β3a and β7 from opposite subunits are colored green. (b) Interactions of the eight-stranded flattened barrel with the major domain. Near the distal splayed corner, the side chains of Tyr23, Lys27, and Arg29 from subunit B (in italics) become projected to the active site of the major domain of subunit A (gray surface, except for atoms closer than 4 Å to the ATP ligands, which are colored green, blue, and white for polar, positively charged, and nonpolar residues, respectively). At the proximal splayed corner, Trp88 is involved in a π-cation interaction with Arg90 and is located next to the N-terminus of α2 from subunit B.

wide-type β-bulge in strand 3 induces a kink of approximately 90°. In this corner, residues Thr31, Ala32, and Pro33 interrupt the regular H-bonding pattern of antiparallel β-strands between β2 and β3b, allowing the N-terminal half, β3a, to form a parallel ladder with β7 from the opposite subunit (Fig. 3a). β3 thus forms part of both sheets and joins them covalently at two diagonally opposite corners, leading to the formation of an eight-stranded flattened barrel (a bimolecular domain). Due to the normal right-handed twist, the two β-sheets are only in contact along the diagonal joining the two covalently linked corners. At the other two corners, the β-sheets splay apart (Fig. 3a). The splayed corner where the eight-stranded flattened barrel domain connects with the major domain is termed the proximal splayed corner, while the other is called the distal splayed corner.

At the proximal splayed corner, Trp88 in the loop linking β5 to β6 contacts N-terminal residues from α2 of the adjacent subunit (Fig. 3b). Trp88 residue is also involved in a π-cation interaction with Arg90 from the same subunit. Since interactions are made with residues from both the major and minor domains, Trp88 serves as a potential fluorescence probe of their relative orientation and other conformational changes, as already described by Guixé *et al.*[22] At the opposite splayed corner, residues Tyr23 and Lys27, together with Arg29 in β3a from one subunit, become oriented towards the active site from the partner subunit of the dimer. Curiously, a molecule of ethylene glycol is observed at the proximal splayed corner of the eight-stranded flattened barrel domain. However, the physiological relevance of this finding, if any, is not clear at the moment.

Both the major and minor domains are involved in the dimer–dimer interface (Fig. 4). That coming from the minor domain involves residues at the distal splayed corner. Specifically, residues 21–24 in the loop connecting β2 to β3a form complementary interactions with residues 99–102 (in the region connecting β6 to β7) of a symmetry-related subunit of the opposite dimer. In the β-meander module of the major domain, two adjacent grooves on either side of the β-sheet (Fig. 4) are involved in the tetramer packing. One groove is lined by residues in the N-terminus of α7. The other groove is formed at the opposite side and includes residues in the loop connecting β13 to α8 and the C-terminal residues in α10.

As seen in Table 2, approximately 1440 Å^2 of surface area is buried at the dimer interface, representing approximately 10% of the total accessible surface area (ASA) of the monomer. A relatively high deviation from the least-squares plane through the atoms of the interface is indicated by the planarity index value[29] of 5.13 of the monomer–monomer interface in contrast with the dimer–dimer interface, which is relatively flat. Nonpolar residues represent almost 68% of the interface and polar residues contribute with 14 H-bonds and no salt bridges. On the other hand, tetramer formation results in the burial of 2154 Å^2 of ASA, representing 8.8% of the dimer surface, with nonpolar residues accounting for almost 59% of this (Table 2).

Interactions with ligands at the active site

Electron density for heteroatoms is observed in the region between the β-meander module in the

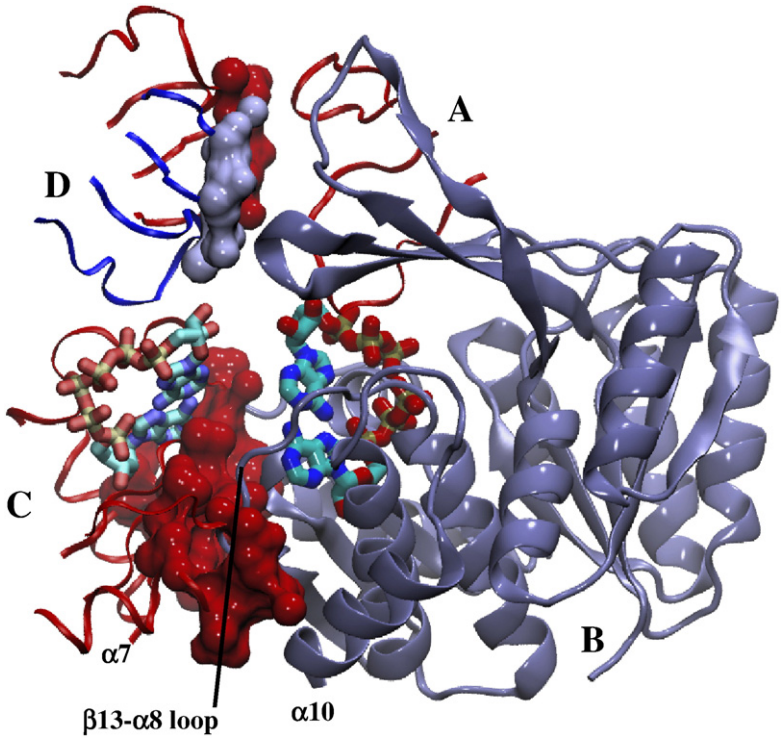

Fig. 4. Interface of association between dimers. Chains are colored according to Fig. 2. In the CD dimer, the accessible surface for a 1.4-Å-radius probe is shown for residues that are within 5 Å of the AB dimer. At the major domain, a groove is formed between the N-terminus of α7 and the central β-sheet. In this cleft, residues from the loop connecting β13 to α8 in subunit B become engaged. Residues from the C-terminus of α10 in B also participate in the interaction. Substrate and allosteric ATP molecules from opposite subunits B and C are shown.

major domain and the distal splayed corner of the orthogonally packed β-sheets. Two ATP molecules and two Mg ions were fitted to this density (Fig. 5).

One ATP is located in a deep groove in the β-meander module of the major domain, surrounded by residues from the N-terminus of α6, the loops connecting β11 to β12 and β13 to α8, the N-terminus of α8, and the C-terminus of α9. Since this location is consistent with the phosphoryl donor site in all the members of the ribokinase-like superfamily, which have known structures for the ligand-bound complex, we call this ATP the substrate ATP. The adenine is stacked by residues at the C-terminus of α9 and the loop connecting β11 to β12. Two water molecules bridge the Watson-Crick edge of the base[30] to main-chain oxygens in the β13–α8 loop. As observed in Fig. 6a, direct interactions to adenine include hydrogen bonds between the side-chain hydroxyl of Ser284 (in α9) and N3 and between that of Ser248 in the β13–α8 loop and the exocyclic nitrogen N6. The ribose moiety is buried in the deepest part of the pocket with the ribosyl ring oxygen (O4′) approaching the interface of helices α8 and α9 and the exocyclic oxygens making direct interactions with protein residues. The O2′ of the ribose forms a bifurcated H-bond with the main-chain O from Val280 and side-chain hydroxyl of Ser284. Interestingly, interactions with Met258 replace the usual Phe stacking of the ribose ring observed in other members of the ribokinase-like superfamily. The triphosphate arm surrounds the N-terminal end of α8. Oxygens in the α-phosphate make hydrogen bonds with the main-chain N from Gly226 and the hydroxyl in the side chain of Ser224 at the C-terminal end of β11. As shown in Fig. 6b, the oxygens of the β-phosphate are engaged in interactions with the side chains of Lys185 and Asn187 from the loop that links β10 to α6. Here, the γ-phosphate becomes oriented towards residues at the N-terminus of α8, particularly Asp256 (see Discussion).

Additional density was modeled as two Mg ions per subunit (Fig. 5), based on the presence of 5 mM $MgCl_2$ in the crystallization setup, the octahedral coordination geometry, and the refined *B*-factors. Oxygens of the β- and γ-phosphates of the substrate ATP are engaged in bidentate coordination with both Mg ions. The side chains of Glu190 and Asp166 make hydrogen bonds with water in the coordination sphere of one of these, which we call the "first Mg". The coordination sphere of the second Mg involves a further bidentate coordination, coming from the β- and γ-phosphates of a second ATP molecule, the allosteric ATP. The remaining coordination positions are occupied by waters, one of which interacts with the side chain of the conserved residue Asn187.

In the case of the allosteric ATP, the region corresponding to the orthophosphate moiety is well defined, as indicated by its *B*-factors. The side-chain amine of Lys27 (from the partner subunit in the dimer) is halfway between the oxygen atoms of the γ-phosphates from both the allosteric and substrate ATPs (Fig. 6b). The side-chain nitrogen of Asn187 interacts with oxygens in the γ-phosphate from the allosteric ATP, while the main-chain nitrogen from Lys27 (partner subunit) is within hydrogen-bonding distance of an oxygen in the β-phosphate and the side chain of Lys189 in α6 interacts with the α-phosphate (Fig. 6b). A network of waters surrounds the triphosphate moiety of the allosteric ATP. Weaker density is observed for the adenine, which shows evidence of presenting two alternative configurations (Fig. 5). In the configuration that presents the strongest density, the Watson-Crick edge of the adenine ring of the allosteric ATP interacts by two hydrogen bonds with the Hoogsteen edge of the substrate ATP, with their glycosidic bonds oriented in *trans*.[30] In the second configuration, the adenine ring is stacked against the aromatic ring of Tyr23 from the partner subunit of the dimer (Fig. 5). No interactions are observed between the

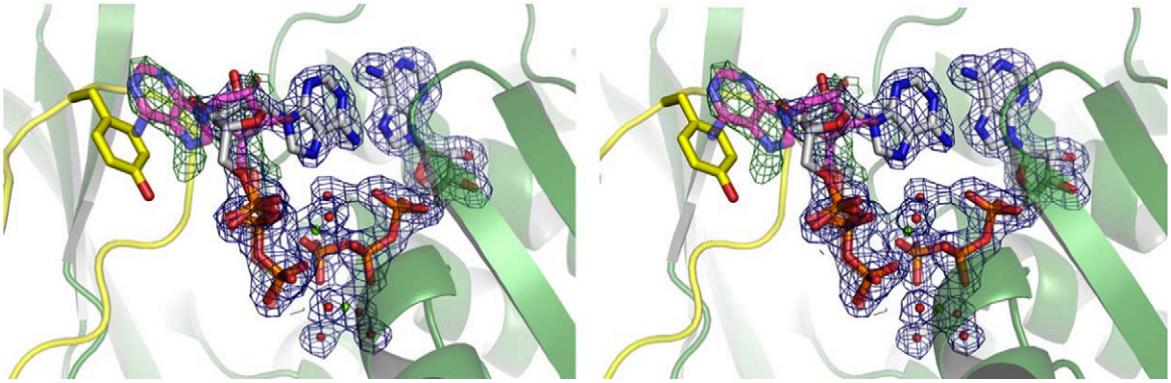

Fig. 5. Stereo view of the $2F_o - F_c$ Fourier electron density map (blue, contoured at 1 σ) of the ligands in subunit A of Pfk-2. The modeled ATP molecules and the Mg ions are represented as white sticks and green balls, respectively. A difference Fourier map (green, contoured at 3 σ) is also shown, suggesting an alternate conformation for the sugar and base moieties of the allosteric ATP (as shown in pink sticks). Nevertheless, the latter is not present in the model, due to inconclusive refinement results. Tyr23, from chain B, is shown in yellow sticks. The figure was prepared using PyMOL [http://www.pymol.org].

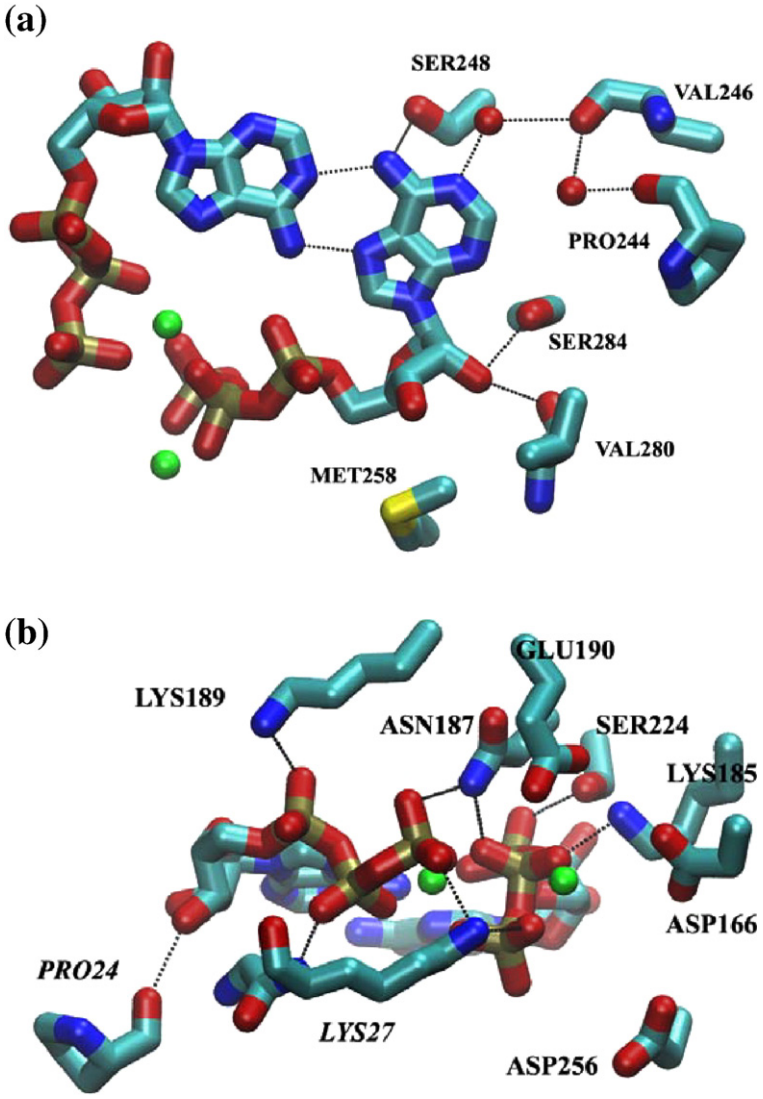

Fig. 6. Interactions with the substrate and allosteric ATPs at the active site of Pfk-2. Dotted lines indicate interatomic distances within 3.5 Å. Water molecules in the coordination sphere of Mg ions (in green) are not shown. (a) Residues surrounding the adenosine moiety of the substrate ATP showing direct and water-mediated interactions; the allosteric ATP is on the left. (b) Residues surrounding the three-phosphate arms of the substrate and allosteric ATPs. Residues coming from the partner subunit in the dimer are in italics.

ATP molecules in one dimer with residues in the facing dimer of the tetramer.

Discussion

The nucleotide binding site in the ribokinase family is mostly accounted for by the β-meander module. Adenine is usually involved in several water-mediated interactions as well as direct interactions with protein residues from the loop emerging from the last strand of the β-meander (β13–α8 loop in Pfk-2). The latter are not generally conserved. Ribose is buried in the deepest part of the binding pocket, between the loop linking the first and second strands of the β-meander and one side of α8 and α9 helices. The triphosphate moiety runs along the groove to the N-terminus of α8, where the γ-phosphate encounters the highly conserved catalytic Asp residue (256 in Pfk-2), which is proposed to abstract the proton from the substrate acceptor, increasing its nucleophilicity in order to attack the γ-phosphate.

As with Pfk-2, Mg ions have been observed in the active sites of homologous structures. In human adenosine kinase, a Mg ion is found in a channel running between the phosphoryl donor and acceptor, with five of its six coordinated waters interacting directly with the protein, for example, with the carboxylate group from Glu226.[13] In the case of AIRs kinase, one Mg is observed bound to the ATP analogue, located between the β- and γ-phosphates and interacting with the oxygen atoms of both.[16] In the case of *Methanocaldococcus jannaschii* nucleoside kinase,[15] a Mg is coordinated octahedrically by six water molecules and is located between adenosine and AMP–PNP in the active site. Waters in the coordination sphere of Mg form hydrogen bonds to the side chains of Asp160, Glu189, and Asp247. In adenosine kinase from *Toxoplasma gondii*, a bound solvent that was designated as a Mg ion does not display the commonly observed octahedral coordination normally seen for Mg and is located between the α- and β-phosphate.[14] The exact nature of this density is therefore dubious. In the active site of *S. aureus* tagatose-6-P kinase, two Mg ions are observed, one coordinated to the γ- and β-phosphates and the other to the β- and α-phosphates of the ATP analogue ATP–PNP. The conserved residue

Fig. 7. Multiple sequence alignment of ribokinase family members. The alignment was obtained after structural superposition of Pfk-2 from *E. coli*, 1-phosphofructokinase from *B. halodurans* (PDB code: 2ABQ), 6-phosphotagatose kinase from *S. aureus* (PDB code: 2JG1), and ribokinase from *E. coli* (PDB code: 1GQT). Secondary-structure elements are indicated for Pfk-2, color coded according to Fig. 1. At a given position, identical residues in the four sequences are shaded black, while identical residues appearing in only three sequences are shaded gray. X indicates undefined residues in the original PDB file. Bold lines indicate the position of the conserved AsnXXGlu motif and the catalytic Asp residue.

Asp163 interacts with the water molecules in the coordination sphere of the first Mg. Thus, the common factor is that in none of the above cases are there protein atoms directly involved in the coordination sphere of the Mg ions. The requirement of two Mg for efficient catalysis in Pfk-2 has been suggested from kinetic experiments together with site-directed mutagenesis of the Glu190 from the AsnXXGlu motif conserved among the members of the ribokinase family[31] (Fig. 7).

Allosteric site and substrate inhibition in Pfk-2

In opposition to Pfk-1, lines of evidence indicate that substrate inhibition in Pfk-2 is a consequence of the binding of the nucleotide to an allosteric site (i.e., different from the active site). The pattern of inhibition by the reaction products and dead-end substrate analogues leads to the conclusion that entrance to the active site is not permissible for MgATP in the absence of fructose-6-P due to a bi–bi ordered sequential mechanism.[21] However, quenching of the intrinsic fluorescence and blue shift of the emission maximum of the single tryptophan of Pfk-2 is observed in the presence of MgATP with no sugar phosphate present,[22] suggesting binding to an allosteric site. The structural changes stabilized by MgATP binding also allow for a change in the oligomerization state of native dimeric Pfk-2 into a tetrameric form with a sigmoidal dependence on the nucleotide concentration.[23] Since the Tyr23Asp mutant is not sensitive to inhibition and is not able to form tetramers,[23] one can deduce that inhibition is the consequence of MgATP binding to an allosteric site, not present in the mutant.

In the structure described here, the allosteric ATP is found in two alternate conformations, with adenine interacting either by Watson-Crick–Hoogsteen hydrogen bonds with the adenine moiety of the substrate ATP or via π-stacking with Tyr23 from the partner subunit of the dimer. The former interaction is uncommon and has, thus far, only been observed in the X-ray structure of a curved RNA helix.[32] The second conformation appears equally interesting. In the Tyr23Asp mutant, the presence of a nonaromatic side chain eliminates the possibility of the π-stacking interaction. Lack of inhibition in this mutant[2] suggests that such an interaction may be critical for the observed reduction in activity at high ATP concentrations, possibly by preventing the binding of the second ATP. Molecular simulation studies together with site-directed mutagenesis are required to better understand the stability of both conformations. The position of the allosteric ATP suggests it to act as a bridge uniting the two domains and favoring the closed conformation. Specifically, the triphosphate moiety simultaneously forms salt bridges with Lys189 from α6 of the major domain and Lys27 from the minor domain of the partner subunit. Additional stabilization comes from the π-stacking interaction with Tyr23 as described above and from interactions between residues from both domains (shown in Fig. 3b).

We have shown previously, using SAXS,[24] that the relative orientation of the domains in the apo form is more open than that in the presence of either fructose-6-P or ATP. If relative domain movements occur during catalysis, the loss of activity at high ATP concentrations may be at least partially understood as a result of stabilizing the closed conformation. Coincidentally, this may simultaneously generate the appropriate dimer–dimer interface for tetramerization, which, via its large interaction surface, would further favor the closed state. Recently, our group has shown that MgATP inhibition persists in the absence of tetramerization in a mutant form of Pfk-2,[33] suggesting that tetramerization is not required for enzyme inhibition.

As the present structure indicates, MgATP inhibition in Pfk-2 is a consequence of the binding of a second ATP to an allosteric site, with part of this site depending on the presence of the substrate ATP, raising the possibility that binding of the allosteric ATP is of an uncompetitive type, according to the Cleland notation.[34] That is, binding of the catalytic ATP is required for the binding of the allosteric one. Furthermore, we can observe that substrate ATP enters the active site in the absence of fructose-6-P, suggesting that a random mechanism should be considered for Pfk-2. Interestingly, in the Tyr23Asp mutant, in which the binding of the allosteric ATP is impaired, ATP can bind to the enzyme in the absence of fructose-6-P (unpublished observations).

The analogous 6-phosphofructokinases from *E. coli*

The term *analogy* is distinguished from *homology* in that the compared characters, although similar, have descended convergently from unrelated ancestral characters.[35] Now that the Pfk-2 structure is available, it is of interest to make some comparisons between the two analogous phosphofructokinases from *E. coli*.

Pfk-1 and Pfk-2 show a core domain with the same architecture (three-layer α/β/α) and a similar topology of the six first strands (the Rossmann arrangement). Cheek *et al.* classified them to the same fold group (the Rossmann-like fold group) in their survey of all available kinase sequences.[36] However, when the Rossmann strands are compared, the third strand in Pfk-1 is antiparallel with the β-sheet and the binding site for the phosphoryl donor occupies different locations in each enzyme (Fig. 8). At the quaternary structural level, two kinds of interfaces are observed in oligomers of both phosphofructokinases. In the case of Pfk-1, one interface holds the active sites while the other holds the allosteric sites. These interfaces have different stabilities; the interactions at the allosteric interface are stronger than the corresponding ones at the active-site interface.[37] The oligomeric state of the wild-type Pfk-1 is not modulated by any known effector.

In the dimeric Pfk-2, the orthogonal packing of the small-domain β-sheet from each monomer (Fig. 3a)

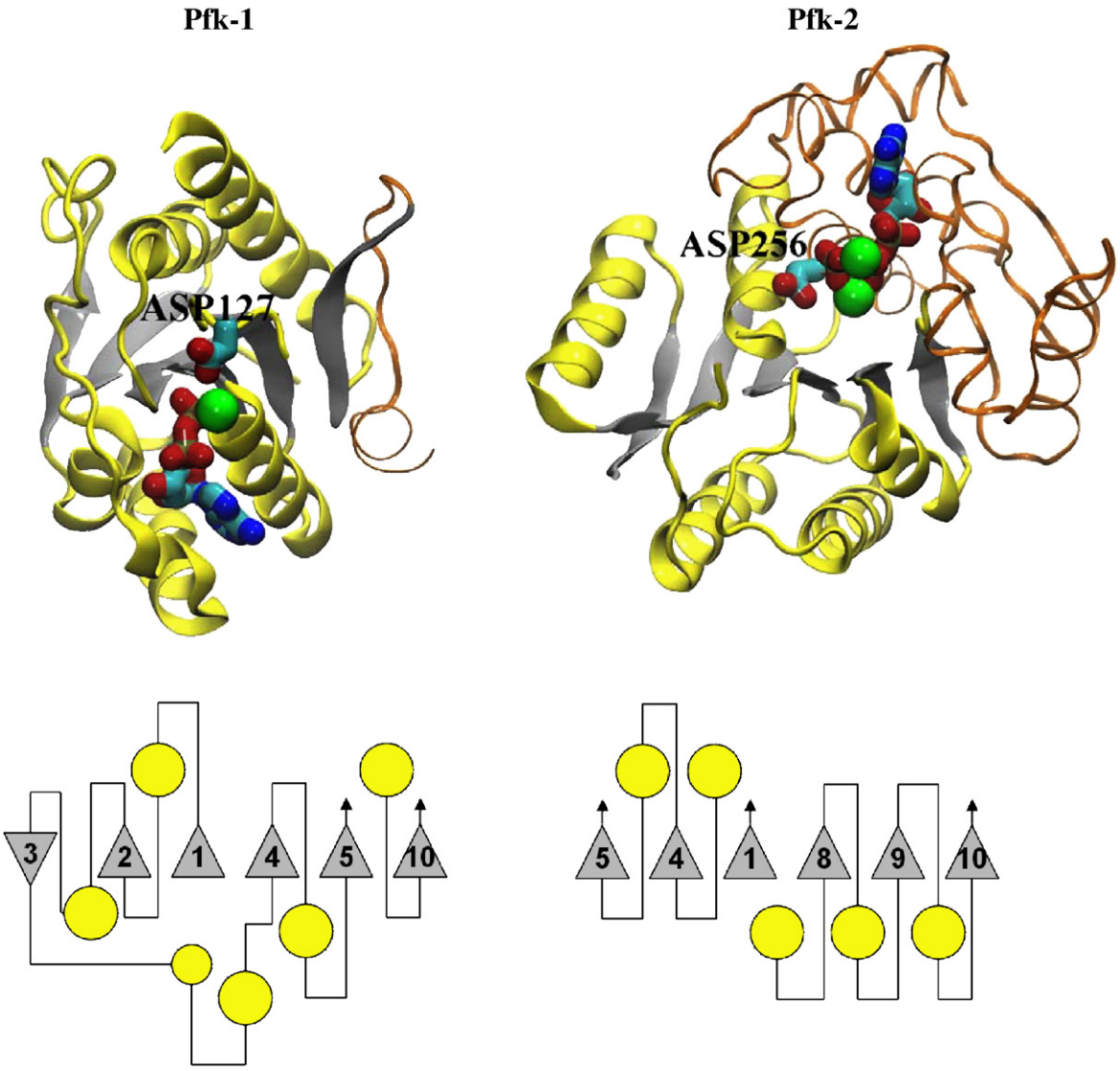

Fig. 8. Analogous structural features in the 6-phosphofructokinases from *E. coli*. The major domains of Pfk-1 and Pfk-2 are shown with the Rossmann strands colored gray and displaying the same relative ordering. The proposed catalytic residues Asp127 in Pfk-1 and Asp256 in Pfk-2 are labeled. The Mg ions and substrate ATP molecules are located at different sites of the corresponding scaffolds. Additional secondary-structure elements at each major domain (the β-meander module in the case of Pfk-2) are shown in orange. Topology diagrams of the Rossmann strands (triangles) and the associated helices (circles) are shown in the lower panel. Broken polypeptide chain is indicated by arrows.

apparently plays a role in the stability of the major domain, since the loss in secondary structure, after dissociation of the dimer by a chaotropic agent, is greater than expected for only the unfolding of the four β-strands.[38]

The second kind of interface in Pfk-2 is regulated by the binding of the allosteric ATP. The packing of two dimers is allowed by the groove formed by α7 in the β-meander module of each monomer (Fig. 4) in which the β13–α8 loop becomes engaged.

In the SAXS modeling study, a tetrameric packing similar to the one observed in the present study gave the best agreement with experimental data but was rejected in favor of a configuration with the active sites looking outward (opposite to that which we observe in this study) since clashes were observed between the major domain regions in the facing dimers.[24] Ribokinase from *E. coli*, whose coordinates were taken as template for homology modeling of Pfk-2, presents slight differences in tertiary structure around the corresponding region.

In Pfk-1, nucleotide binding at the active site includes interactions with the β-phosphate, hydrophobic contacts and hydrogen bonds to the hydroxyls of the ribose, and hydrophobic interactions with adenine.[5] Site-directed mutagenesis studies[39] highlight the role of Arg82 and Arg111 as determinants of nucleotide specificity in Pfk-1. In terms of catalysis, Asp127 plays a critical role as a general base, increasing the nucleophilicity of the 1-hydroxyl of fructose-6-P by abstracting its proton and permitting attack on the γ-phosphate of the substrate ATP. During this process, a pentacoordinated γ-phosphate transition state may be stabilized by

Table 1. Data collection parameters and structure refinement statistics

Data collection	
Space group	$P222_1$
Cell parameters (Å)	$a=42.8$, $b=86.8$, $c=171.3$
Resolution range (Å)	20.0–1.98 (2.09–1.98)
Unique reflections	43,478 (5514)
Redundancy	5.8 (5.3)
R_{sym} (%)	7.5 (30.2)
Completeness (%)	93.8 (90.1)
$I/\sigma(I)$	18.6 (4.3)
Molecules/AU	2
Solvent content (%)	49.8
Matthews coefficient (A^3/Da)	2.46
Refinement	
R-factor/R_{free} (%)	18.6/23.4
Average B-factor/r.m.s.d. (Å^2)	
Main chain (612 residues)	22.4/0.8
Side chain (482 residues)	25.6/1.6
ATP (4 molecules)	17.4/2.4
Mg (4 ions)	12.4/0.7
Solvent (463 molecules)	25.6/9.0
Refinement (r.m.s.d. from standard geometries)	
Bond length (Å)	0.011
Bond angles (°)	1.483
Ramachandran plot (%)	
Most favored	98.5
Allowed	1.0
Outliers	0.5

Values in parentheses are for the outer-resolution shells.

several groups including the side chains of Arg72 and Arg171.[40] By homology with other known ribokinase-like superfamily members, Asp256 in Pfk-2 can be inferred to be the analogue of Asp127 in Pfk-1. Unlike Asp127, which is located in the loop following the fifth Rossmann strand in Pfk-1, Asp256 in Pfk-2 is located in α8 within the β-meander module (Fig. 8).

During catalysis by Pfk-1, the single Mg ion observed in its structure[5] is proposed to establish critical interactions for transition state stabilization. The acidic residues Asp103 and Asp129 are involved in direct and water-mediated interactions with the single Mg, respectively. With the binding of a second Mg in Pfk-2, a net charge of 0 is obtained for the metal–nucleotide complex, facilitating the effective attack by the activated hydroxyl from the substrate. At present, it is difficult to draw definitive conclusions concerning the reaction mechanism in terms of the crystal structure given that the sugar substrate is absent from the complex. Nevertheless, it would appear that at least some of the structural features necessary for catalysis in Pfk-1 have analogous counterparts in Pfk-2 and that the chemistry of the reaction probably differs in the use of Mg.

Finally, a possible suggestion of nonredundant function of Pfk-1 and Pfk-2 from *E. coli* comes from metabolic flux ratio analysis of a knockout mutant defective in Pfk-1.[41] Although a low growth rate on glucose was observed, a significant increase in the flux partitioning through the pentose–phosphate pathway occurs, suggesting that the intact Pfk-2 is preferentially channeling fructose-P produced by this pathway towards the lower part of glycolysis. This idea is congruent with the original proposal by Ureta[42] about the role of isozymes in the channeling of flux through different pathways that have common activities as one possible functional meaning of redundancy of enzymatic activity, a curiously widespread phenomenon in metabolism.

Experimental Procedures

Crystallization, data collection, and processing

The steps involved in recombinant protein production, crystallization, and data collection have been described previously.[25] Crystallization experiments were performed at 18 °C using the conventional hanging-drop vapor-diffusion technique. Before data collection at cryogenic temperature (100 K), crystals were soaked with a cryoprotectant solution containing 25% ethylene glycol diluted in mother liquor and subsequently flash frozen. A substantially complete X-ray diffraction data set up to 1.98 Å resolution was obtained at the Brazilian Synchrotron Light Source (Laboratorio Nacional de Luz Sincrotron, Campinas, SP) beamline MX1 (λ = 1.438 Å) on a MAR CCD detector, with a crystal-to-detector distance of 90 mm and oscillation steps of 1°. Raw data images were processed with MOSFLM,[43] scaled, and merged with SCALA,[44] and amplitudes were estimated using TRUNCATE.[45]

Phasing and model refinement

The first set of phases was obtained by means of the molecular replacement technique as implemented in the program Phaser,[46] searching for two monomers in the asymmetric unit, as predicted from the Matthews coefficient of $V_M=2.46$ Å^3/Da (corresponding to a solvent content of 49.8 %). A monomer of 1-phosphofructokinase (31% sequence identity) from *B. halodurans* was used as the search model (PDB code: 2ABQ).

Rigid-body refinement and simulated annealing refinement were performed on 95% of the data using CNS,[47] followed by subsequent cycles of positional and *B*-factor refinement carried out with REFMAC.[48] R_{free} was calculated on the basis of the remaining 5%. Real-space refinement, including Fourier electron density map inspection, was performed with Coot.[49] Noncrystallographic symmetry restraints were used up until the final stages of TLS refinement. Solvent water molecules, treated as oxygen atoms, were added using the appropriate Coot routine. During the model refinement, the inspection of Fourier difference maps indicated the presence of very strong non-protein electron densities (more than 4σ in height) in each

Table 2. Structural analysis on the interfaces of Pfk-2

Protein interface parameters	Between monomers along *p*-axis	Between dimers along *q*-axis
Interface ASA (Å^2)	1444	2154
Percentage of ASA	10.5	8.8
Planarity (Å)	5.13	3.17
Length/Breadth (Å)	34.32/35.45	75.12/38.38
Percentage of polar atoms in interface	32	41.1
Percentage of nonpolar atoms in interface	67.9	58.9
Hydrogen bonds	14	4

monomer of the asymmetric unit inside the canonical active site. Due to their size and shape, they were readily identified as ATP molecules and magnesium ions and subsequently refined as such. The overall stereochemical quality of the final model and the agreements between model and experimental data were assessed by both the program PROCHECK[50] and the appropriate Coot routines.

Structure determination

The final model was refined until convergence of the reliability indices to 18.5% (*R*-factor) and 23.3% (R_{free}) and consists of two copies of the Pfk-2 monomer in the asymmetric unit, 4 molecules of ATP (two per monomer), 4 magnesium ions, and 463 water molecules. We refer to the two monomers of the asymmetric unit as the dimer, which is composed of subunits A and B. In the final structure, 98.5% of residues were in the most favorable regions of the Ramachandran plot, 1% in additionally allowed regions, and the remaining 0.5% as outliers, but in conformations explained by clear electron density. Data collection, refinement, and quality parameters as well as the statistics for the final model are summarized in Table 1. The best refinement results were reached by using elevated noncrystallographic symmetry weights at the beginning of the procedure, followed by a stepwise relaxation, until complete elimination of such. Evidence for local flexibility and interdomain motions was analyzed by the TLSMD server,[51] and optimal TLS group definitions were applied at the end of the refinement protocol. The electron density around one of the two ATP molecules per monomer (described above as the allosteric ATP) suggested the possibility of two alternative orientations for the adenine moiety. However, it proved difficult to reliably attribute occupancies for both. The deposited coordinates therefore correspond to the most clearly defined conformation.

The r.m.s.d., calculated by LSQMAN,[52] after superposing all C^{α} atoms between the two monomers, was 0.36 Å (with a maximum deviation of 1.32 Å). Minor differences are observed between the monomers in the asymmetric unit, most notably five missing residues in a loopy region close to the C-terminus of chain A (residues 289–293), which are present in chain B.

Structural description

The interfacial parameters shown in Table 2 were calculated at the Protein–Protein Interaction Server†. Images were generated using VMD[53] and PyMOL‡.

PDB accession code

Atomic coordinates and structure factors have been deposited in the PDB with the accession code 3CQD.

Acknowledgements

This work was supported by a grant from the Comisión Nacional de Investigación Científica y Tecnológica, FONDECYT 1050818. R.C.G. and A.L. B.A. thank Fundação de Amparo à Pesquisa do Estado de São Paulo for financial support via the Centros de Pesquisa, Inovação e Difusão program to Centro de Biotecnologia Molecular Estrutural. We thank Dr. Mauricio Baez for useful discussions.

† www.biochem.ucl.ac.uk/bsm/PP/server/
‡ www.pymol.org

References

1. Portais, J. C. & Delort, A. M. (2002). Carbohydrate cycling in micro-organisms: what can (13)C-NMR tell us? *FEMS Microbiol. Rev.* **26**, 375–402.
2. Guixé, V. & Babul, J. (1985). Effect of ATP on phosphofructokinase-2 from *Escherichia coli*. A mutant enzyme altered in the allosteric site for MgATP. *J. Biol. Chem.* **260**, 11001–11005.
3. Zheng, R. L. & Kemp, R. G. (1992). The mechanism of ATP inhibition of wild type and mutant phospho-fructo-1-kinase from *Escherichia coli*. *J. Biol. Chem.* **267**, 23640–23645.
4. Torres, J. C., Guixé, V. & Babul, J. (1997). A mutant phosphofructokinase produces a futile cycle during gluconeogenesis in *Escherichia coli*. *Biochem. J.* **327**, 675–684.
5. Shirakihara, Y. & Evans, P. R. (1988). Crystal structure of the complex of phosphofructokinase from *Escherichia coli* with its reaction products. *J. Mol. Biol.* **204**, 973–994.
6. Rypniewski, W. R. & Evans, P. R. (1989). Crystal structure of unliganded phosphofructokinase from *Escherichia coli*. *J. Mol. Biol.* **207**, 805–821.
7. Lau, F. T. & Fersht, A. R. (1989). Dissection of the effector-binding site and complementation studies of *Escherichia coli* phosphofructokinase using site-directed mutagenesis. *Biochemistry*, **28**, 6841–6847.
8. Johnson, J. L. & Reinhart, G. D. (1992). MgATP and fructose 6-phosphate interactions with phosphofructokinase from *Escherichia coli*. *Biochemistry*, **31**, 11510–11518.
9. Deville-Bonne, D., Laine, R. & Garel, J. R. (1991). Substrate antagonism in the kinetic mechanism of *E. coli* phosphofructokinase-1. *FEBS Lett.* **290**, 173–176.
10. Wang, X. & Kemp, R. G. (2001). Reaction path of phosphofructo-1-kinase is altered by mutagenesis and alternative substrates. *Biochemistry*, **40**, 3938–3942.
11. Bork, P., Sander, C. & Valencia, A. (1993). Convergent evolution of similar enzymatic function on different protein folds: the hexokinase, ribokinase, and galactokinase families of sugar kinases. *Protein Sci.* **2**, 31–40.
12. Sigrell, J. A., Cameron, A. D., Jones, T. A. & Mowbray, S. L. (1998). Structure of *Escherichia coli* ribokinase in complex with ribose and dinucleotide determined to 1.8 Å resolution: insights into a new family of kinase structures. *Structure*, **6**, 183–193.
13. Mathews, I. I., Erion, M. D. & Ealick, S. E. (1998). Structure of human adenosine kinase at 1.5 Å resolution. *Biochemistry*, **37**, 15607–15620.
14. Schumacher, M. A., Scott, D. M., Mathews, I. I., Ealick, S. E., Roos, D. S., Ullman, B. & Brennan, R. G. (2000). Crystal structures of *Toxoplasma gondii* adenosine kinase reveal a novel catalytic mechanism and prodrug binding. *J. Mol. Biol.* **296**, 549–567.
15. Arnfors, L., Hansen, T., Schonheit, P., Ladenstein, R. & Meining, W. (2006). Structure of *Methanocaldococcus jannaschii* nucleoside kinase: an archaeal member of the ribokinase family. *Acta Crystallogr., Sect. D: Biol. Crystallogr.* **62**, 1085–1097.

16. Zhang, Y., Dougherty, M., Downs, D. M. & Ealick, S. E. (2004). Crystal structure of an aminoimidazole riboside kinase from *Salmonella enterica*: implications for the evolution of the ribokinase superfamily. *Structure*, **12**, 1809–1821.
17. Ohshima, N., Inagaki, E., Yasuike, K., Takio, K. & Tahirov, T. H. (2004). Structure of *Thermus thermophilus* 2-keto-3-deoxygluconate kinase: evidence for recognition of an open chain substrate. *J. Mol. Biol.* **340**, 477–489.
18. Mathews, I. I., McMullan, D., Miller, M. D., Canaves, J. M., Elsliger, M. A., Floyd, R. *et al.* (2008). Crystal structure of 2-keto-3-deoxygluconate kinase (TM0067) from *Thermotoga maritima* at 2.05 Å resolution. *Proteins*, **70**, 603–608.
19. Miallau, L., Hunter, W. N., McSweeney, S. M. & Leonard, G. A. (2007). Structures of *Staphylococcus aureus* D-tagatose-6-phosphate kinase implicate domain motions in specificity and mechanism. *J. Biol. Chem.* **282**, 19948–19957.
20. Berman, H. M., Battistuz, T., Bhat, T. N., Bluhm, W. F., Bourne, P. E., Burkhardt, K. *et al.* (2002). The Protein Data Bank. *Acta Crystallogr., Sect. D: Biol. Crystallogr.* **58**, 899–907.
21. Campos, G., Guixé, V. & Babul, J. (1984). Kinetic mechanism of phosphofructokinase-2 from *Escherichia coli*. A mutant enzyme with a different mechanism. *J. Biol. Chem.* **259**, 6147–6152.
22. Guixé, V., Rodríguez, P. H. & Babul, J. (1998). Ligand-induced conformational transitions in *Escherichia coli* phosphofructokinase-2: evidence for an allosteric site for $MgATP^2$. *Biochemistry*, **37**, 13269–13275.
23. Guixé, V. & Babul, J. (1988). Influence of ligands on the aggregation of the normal and mutant forms of phosphofructokinase-2 of *Escherichia coli*. *Arch. Biochem. Biophys.* **264**, 519–524.
24. Cabrera, R., Fischer, H., Trapani, S., Craievich, A. F., Garratt, R. C., Guixé, V. & Babul, J. (2003). Domain motions and quaternary packing of phosphofructokinase-2 from *Escherichia coli* studied by small angle x-ray scattering and homology modeling. *J. Biol. Chem.* **278**, 12913–12919.
25. Cabrera, R., Caniuguir, A., Ambrosio, A. L., Guixé, V., Garratt, R. C. & Babul, J. (2006). Crystallization and preliminary crystallographic analysis of the tetrameric form of phosphofructokinase-2 from *Escherichia coli*, a member of the ribokinase family. *Acta Crystallogr., Sect. F: Struct. Biol. Cryst. Commun.* **62**, 935–937.
26. Richardson, J. S., Getzoff, E. D. & Richardson, D. C. (1978). The beta bulge: a common small unit of nonrepetitive protein structure. *Proc. Natl Acad. Sci. USA*, **75**, 2574–2578.
27. Caniuguir, A., Cabrera, R., Baez, M., Vásquez, C. C., Babul, J. & Guixé, V. (2005). Role of Cys-295 on subunit interactions and allosteric regulation of phosphofructokinase-2 from *Escherichia coli*. *FEBS Lett.* **579**, 2313–2318.
28. Chothia, C. & Janin, J. (1982). Orthogonal packing of beta-pleated sheets in proteins. *Biochemistry*, **21**, 3955–3965.
29. Jones, S. & Thornton, J. M. (1996). Principles of protein–protein interactions. *Proc. Natl Acad. Sci. USA*, **93**, 13–20.
30. Leontis, N. B., Stombaugh, J. & Westhof, E. (2002). The non-Watson-Crick base pairs and their associated isostericity matrices. *Nucleic Acids Res.* **30**, 3497–3531.
31. Parducci, R. E., Cabrera, R., Baez, M. & Guixé, V. (2006). Evidence for a catalytic Mg^{2+} ion and effect of phosphate on the activity of *Escherichia coli* phosphofructokinase-2: regulatory properties of a ribokinase family member. *Biochemistry*, **45**, 9291–9299.
32. Baeyens, K. J., De Bondt, H. L., Pardi, A. & Holbrook, S. R. (1996). A curved RNA helix incorporating an internal loop with G.A and A.A non-Watson-Crick base pairing. *Proc. Natl Acad. Sci. USA*, **93**, 12851–12855.
33. Baez, M., Merino, F., Astorga, G. & Babul, J. (2008). Uncoupling the MgATP-induced inhibition and aggregation of *Escherichia coli* phosphofructokinase-2 by C-terminal mutations. *FEBS Lett.* **582**, 1907–1912.
34. Cleland, W. W. (1963). The kinetics of enzyme-catalyzed reactions with two or more substrates or products. II. Inhibition: nomenclature and theory. *Biochim. Biophys. Acta*, **67**, 104–137.
35. Fitch, W. M. (2000). Homology. A personal view on some of the problems. *Trends Genet.* **16**, 227–231.
36. Cheek, S., Ginalski, K., Zhang, H. & Grishin, N. V. (2005). A comprehensive update of the sequence and structure classification of kinases. *BMC Struct. Biol.* **5**, 6.
37. Deville-Bonne, D., Le Bras, G., Teschner, W. & Garel, J. R. (1989). Ordered disruption of subunit interfaces during the stepwise reversible dissociation of *Escherichia coli* phosphofructokinase with KSCN. *Biochemistry*, **28**, 1917–1922.
38. Baez, M., Cabrera, R., Guixé, V. & Babul, J. (2007). Unfolding pathway of the dimeric and tetrameric forms of phosphofructokinase-2 from *Escherichia coli*. *Biochemistry*, **46**, 6141–6148.
39. Wang, X. & Kemp, R. G. (1999). Identification of residues of *Escherichia coli* phosphofructokinase that contribute to nucleotide binding and specificity. *Biochemistry*, **38**, 4313–4318.
40. Berger, S. A. & Evans, P. R. (1992). Site-directed mutagenesis identifies catalytic residues in the active site of *Escherichia coli* phosphofructokinase. *Biochemistry*, **31**, 9237–9242.
41. Fischer, E. & Sauer, U. (2003). Metabolic flux profiling of *Escherichia coli* mutants in central carbon metabolism using GC–MS. *Eur. J. Biochem.* **270**, 880–891.
42. Ureta, T. (1991). The role of isozymes in metabolite channeling. *J. Theor. Biol.* **152**, 81–84.
43. Leslie, A. G. W. (1992). Recent changes to the MOSFLM package for processing film and image plate data. *Joint CCP4+ESF-EAMCB Newsletter on Protein Crystallography*, **26**.
44. Evans, P. R. (1993). Data reduction. In *Data Collection and Processing: Proceedings of the CCP4 Study Weekend* (Sawyer, L., Isaacs, N. & Bailey, S., eds), pp. 114–122, Daresbury Laboratory, Warrington, UK.
45. French, G. S. & Wilson, K. S. (1978). On the treatment of negative intensity observations. *Acta Crystallogr., Sect. A: Cryst. Phys., Diffr., Theor. Gen. Crystallogr.* **34**, 517–525.
46. McCoy, A. J., Grosse-Kunstleve, R. W., Adams, P. D., Winn, M. D., Storoni, L. C. & Read, R. J. (2007). Phaser crystallographic software. *J. Appl. Crystallogr.* **40**, 658–674.
47. Brunger, A. T., Adams, P. D., Clore, G. M., DeLano, W. L., Gros, P., Grosse-Kunstleve, R. W. *et al.* (1998). Crystallography and NMR system: a new software suite for macromolecular structure determination. *Acta Crystallogr., Sect. D: Biol. Crystallogr.* **54**, 905–921.
48. Murshudov, G. N., Vagin, A. A. & Dodson, E. J. (1997). Refinement of macromolecular structures by the maximum-likelihood method. *Acta Crystallogr., Sect. D: Biol. Crystallogr.* **53**, 240–255.
49. Emsley, P. & Cowtan, K. (2004). Coot: model-building tools for molecular graphics. *Acta Crystallogr., Sect. D: Biol. Crystallogr.* **60**, 2126–2132.
50. Laskowski, R. A., MacArthur, M. W., Moss, D. S. & Thornton, J. M. (1993). PROCHECK: a program to

check the stereochemical quality of protein structures. *J. Appl. Crystallogr.* **26**, 283–291.
51. Painter, J. & Merritt, E. A. (2006). TLSMD server for the generation of multi-group TLS models. *J. Appl. Crystallogr.* **39**, 109–111.
52. Kleywegt, G. J. & Jones, T. A. (1994). A super position. *CCP4/ESF-EACBM Newsletter on Protein Crystallography*, **31**, 9–14.
53. Humphrey, W., Dalke, A. & Schulten, K. (1996). VMD: visual molecular dynamics. *J. Mol. Graphics*, **14**, 33–38.